Effect of skin fracture on failure of a bilayer polymer structure

Marie-Aude Godart and Patrick Leevers

Department of Mechanical Engineering, Imperial College London, London SW7 2AZ, UK

Abstract

A thin skin of low tensile failure strain, if bonded to the tensile surface of an un-notched impact bend specimen of much tougher material, can change the global failure mode from ductile to brittle. A novel model of this well-known effect is developed and applied to results from impact tests on a tough core of polyamide-polyethylene blend, with a single skin of brittle EVOH. At a fixed crosshead speed, notched specimens of the blend become brittle at a relatively low temperature T_{bt}. Un-notched bilayer specimens continue to show skin fracture up to a considerably higher temperature T_{fs}; above this temperature they do not fail at all but below T_{bt} they too fail in a brittle manner. Within the temperature range from T_{fs} down to T_{bt} there is a transition from crack arrest, either at the skin/core interface or further into the core where a crack would not normally propagate, to brittle fracture. This brittle fracture temperature is predicted by modelling the process as a three-phase impact event. In the first phase, the striker bends the bilayer quasi-statically. The second phase begins with instantaneous fracture of the skin at its failure strain. The skin ends retract at finite speed, and a craze grows in the adjacent core material to accommodate the local strain singularity. The last phase is a striker-driven impact event similar to that in a *notched* bend specimen of the core material, except that the crack-tip craze already bears the adiabatic temperature distribution generated while it was driven open by skin retraction. The criterion for craze decohesion, and hence for a crack jump, is the same adiabatic decohesion criterion which accounts for the speed-dependence of impact fracture in notched monolayer specimens. Applied computationally, this model predicts whether a bilayer structure fails in a brittle way or whether cracks initiated in the skin are arrested, either temporarily or permanently, at the skin/core interface.

Key words: Adiabatic decohesion, crack arrest, fracture mechanisms, impact TPB tests, polymeric bilayer material, rapid crack propagation, surface embrittlement

Nomenclature

β	Thermomechanical efficiency
ΔH_{f}	Latent heat of fusion
δ	Crack tip opening displacement (COD)
δ_{F}	COD when the crack opening rate of the skin retraction phase reaches zero in the finite volume program
δ_{r}	COD at the crack tip in the remote loading configuration
δ_{u}	Crack opening displacement at the crack tip in the uniform loading configuration
$\dot{\delta}$	Crack tip opening rate
$\dot{\delta}_0$	Initial crack opening rate of the skin retraction phase in the finite volume program
ϵ_{fs}	Failure strain
κ	Thermal diffusivity
λ_{F}	Fibril draw ratio
ρ	Mass density
ρ^*	Relative craze density
σ_{c}	Cohesive stress or craze stress
σ_{r}	Remote stress
σ_{u}	Uniform normal cohesive traction
a	Crack length
B	Thickness of a TPB specimen
C	Load point compliance
c	Craze length
C^*	Non dimensional compliance
c_0	Longitudinal wave speed
C_{p}	Specific heat
d	Displacement of the striker on a TPB specimen
E	Young's modulus
E_{sec}	Secant modulus
F	Load measured during a TPB test
h	Surface heat transfer coefficient
j	Finite volume cell number
k	Thermal conductivity
K_{Ir}	Stress intensity factor in the remote loading configuration
K_{Iu}	Stress intensity factor in the uniform stress configuration
L	Length of a TPB specimen
L_0	Cell size of finite volume model
q''	Rate of heat generated per unit area
$r(a)$	Geometry function of the stress intensity factor in the remote loading configuration
S	Span of a TPB specimen
s	Skin thickness of a bilayer specimen
s_{c}	Critical thickness of the melt layer in the adiabatic decohesion model

T Temperature
t Time
T_0 Initial test temperature
T_{bts} Transition temperature of a bilayer structure between the brittle and permanent arrest fracture modes
T_{bt} Brittle/ductile transition temperature
t_{dc} Failure time predicted by the adiabatic decohesion model
T_{fs} Temperature of failure of the skin of a bilayer structure
T_{m} Melting temperature
$u(c,a)$ Geometry function of the stress intensity factor in the uniform stress configuration
W Width of a TPB specimen
Fo Fourier number

1 Introduction

The deleterious effect of a skin material on the mechanical properties of a core material is a problem encountered in many different situations. Coatings intended to fulfil specific functions such as decoration, mechanical protection, diffusion barrier or electrical insulation) were studied by Kim and Nairn (2000). The ability of a bilayer structure to initiate brittle fracture has also been exploited for the purposes of research on rapid crack propagation (Ivankovic (1991)), arrest (Theocaris and Milios (1981)), or the interface effects in composite materials (Cudre-Mauroux et al. (1991)). A distinct skin may be formed unintentionally, e.g. when the surface material is modified by environmental ageing or by shear in injection moulding. In the first case, a brittle layer forms at the surface due to oxidation, ultraviolet radiation, exposure to elevated temperature, or stress cracking agents (Schoolenberg and Meijer (1991)). Injection moulding may form skin layers which are more rigid and tougher in the flow direction than the core material.

In many situations, it has been observed that the presence of the skin *embrittles* the core material: skinned structures fail under conditions in which similar un-skinned structures do not. Various approaches have been used to study this effect, depending on the direction of crack propagation relative to the skin and on the presence or absence of an initial notch and/or of an adhesive interlayer. This paper investigates and models a crack which propagates from a brittle layer, with a low failure strain, to a tougher and less rigid core, the propagation direction being perpendicular to the interface plane. The presence of the skin in this case has been compared to that of a notch, as deep as the skin thickness, in a monolayer core specimen. Many authors, such as Djiauw and Fesko (1976) found that with

a thick skin and/or at high deformation rate, the effect of a skin was more embrittling than that of a notch. While embrittlement had been observed by many authors, few agree on its mechanism; it has been attributed to the restriction of crazing in the core (So and Broutman (1982)), the high elastic energy stored in the skin (Djiauw and Fesko (1976) and Cudre-Mauroux et al. (1991)), the poor viscoelastic properties of the skin (Verpy et al. (1994)), the elastic property discontinuity of the interface (Theocaris and Milios (1981)) and the effect of high strain rate on the brittle/ductile transition of the core material (Konczol et al. (1991)) as the crack meets the interface.

The core material studied here is the polyamide-based thermoplastic alloy Orgalloy®and the skin is an ethylene vinyl alcohol copolymer (EVOH) which has excellent barrier properties but a low failure strain of 2-5% at -40°C and 5 s^{-1}. There is no adhesive layer between skin and core and strong skin-core adhesion prevents delamination at the interface. The fracture properties are investigated using three-point bending (TPB) tests: a striker hits the face opposite the un-notched skin at specified crosshead speed and temperature conditions.

2 Fracture modes of bilayer structures

TPB tests were carried out on impact bend specimens with a width W of 4 mm, a thickness B of 10 mm, a length L of 48 mm and a span S of 40 mm. Materials were prepared by hot pressing EVOH films of 0.1, 0.3 and 0.6 mm thickness s onto rubber-toughened (referred as toughened bilayer) and untoughened Orgalloy (referred as un-toughened bilayer) plates. The specimens were tested using an Instron VHS high rate machine at a crosshead speed of 1 m/s. The load and displacement histories were measured using a Kistler piezoelectric load cell and the built-in Linear Variable Displacement Transducer, and were captured using an oscilloscope. A liquid nitrogen cooled chamber was used to set each test temperature in the range -20 to 20°C.

Firstly, in order to highlight the effect of the skin, TPB tests with the striker hitting the face opposite the EVOH layer were compared with similar tests with the striker hitting directly the EVOH layer. Figure 1 illustrates that tensile fracture of the EVOH layer was responsible for failure of the specimens.

Four different types of load-displacement trace were obtained for the bilayer structures, depending on material properties and on the TPB test conditions (Fig. 2). Brittle behaviour was observed at low temperatures

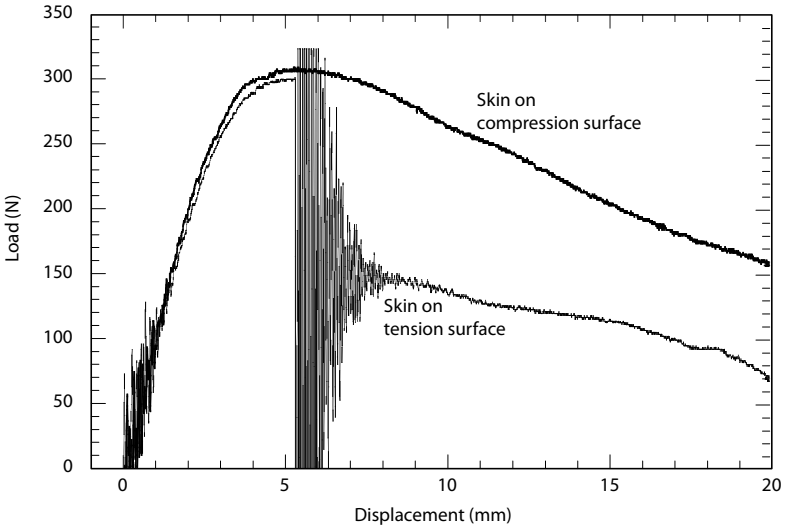

Fig. 1. Load-displacement traces for toughened bilayer specimens with 0.6 mm of EVOH at 20°C (for higher displacements, the load decreases steadily to zero).

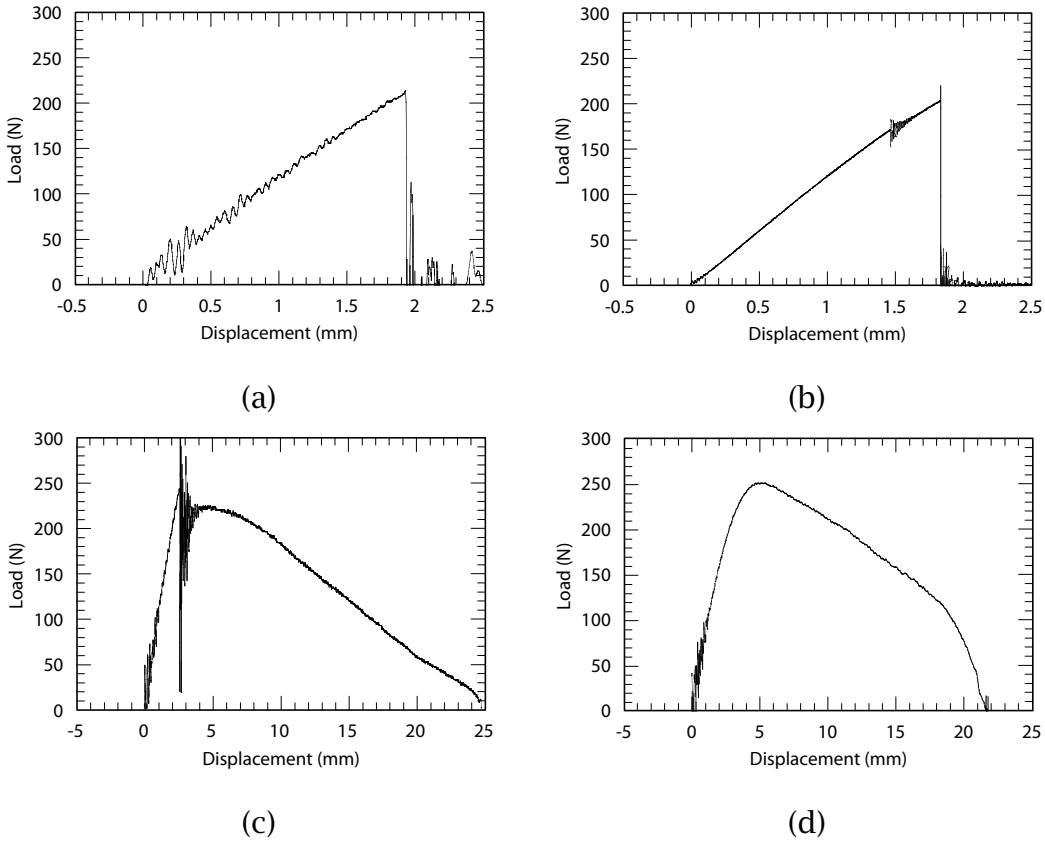

Fig. 2. Load-displacement traces illustrating different fracture modes observed in TPB bilayer specimens: (a) brittle, (b) temporary arrest followed by RCP, (c) permanent arrest, (d) bending.

and/or high strain rates (Fig. 2a). The load-displacement trace was approximately triangular or showed some non-linearity during loading. Rapid crack propagation (RCP) then caused rapid unloading.

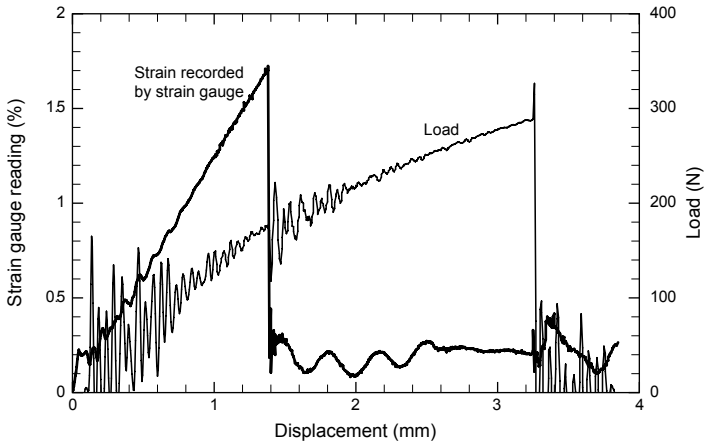

Fig. 3. Load-displacement for an un-toughened bilayer specimen with 0.1 mm of EVOH at 0°C and 1 m/s. A strain gauge was glued on the EVOH layer, and the strain values are shown in the graph.

At higher temperatures and/or lower strain rates, other fracture modes were observed. The initial part of the signal remained similar to the brittle case, but RCP then arrested (Fig. 2b and 2c). Figure 3 shows that a strain gauge fixed on the EVOH surface broke during unloading, proving that a crack had initiated. In the situation of Fig. 2b, the arrest was temporary and the crack reinitiated later provoking failure by RCP, whereas in the situation of Fig. 2c, the arrest was permanent — the specimen remained partly cracked but in one piece. In the final failure mode there was no RCP (Fig. 2d). The load-displacement trace shows no sharp drop; after the load reaches a maximum it decreases monotonically. In this case there was no slow crack growth either, although the resulting trace looks similar to that of ductile fracture; the specimen was just bent, and no cracks were formed.

The next few paragraphs explore the effects of skin thickness, skin properties and core properties on the failure mode.

2.1 Effect of skin thickness and properties

For ratios of skin thickness to total specimen width from 0.025 to 0.15, skin thickness did not affect the fracture mode in bilayer specimens at any given temperature and crosshead speed, whereas notch size — of similar size to the skin thickness — did so in Orgalloy monolayer specimens. This confirms that the effect of the skin is not equivalent to that of a notch.

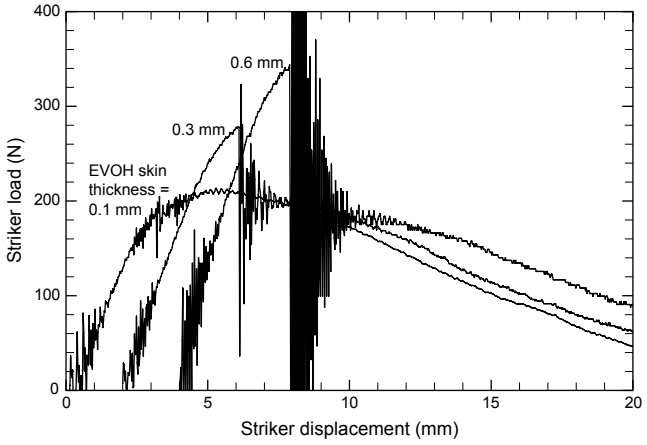

Fig. 4. Load-displacement traces for the toughened bilayer with EVOH skins of various thicknesses at 20°C (for higher displacement the load just falls steadily to zero).

Under conditions in which arrest occurred (Fig. 2b and 2c), the crack jump distance before arrest did depends on the skin thickness: the thicker the skin the further the crack propagated.

For thin skins, multiple cracks formed and arrested at the interface. This phenomenon has been observed by So and Broutman (1982), Djiauw and Fesko (1976), Kim and Nairn (2000) and others. As well as being directly visible on the specimen fracture surface, multiple initiation events could also be seen on the load-displacement traces (Fig. 4). The further each crack jumps, the greater is the unloading on the load-displacement trace.

Failure properties of four EVOH grades in different skin thicknesses were investigated using TPB tests on bilayer structures. The transition from bending failure to fracture was attributed to failure of the EVOH skin at a temperature denoted T_{fs}. The skin is assumed to fail when the surface strain of the bilayer specimen reaches a characteristic failure strain and this was determined both from the load-displacement traces — either at the final displacement for brittle specimens or at the point of unloading when arrest occurred — and using strain gauges fixed on the EVOH skin (Fig. 3). A value of 3% was found and is assumed to be independent of temperature at −20, 0 and 20°C.

2.2 Effect of core properties

The properties of the core material were observed to have a very strong influence on the fracture mode of a bilayer structure. Permanent arrest in the core material was observed only for rubber-toughened Orgalloy, while temporary arrest was observed only for un-toughened Orgalloy and

then only at the interface (for a low EVOH thickness). The brittle/ductile transition temperature of the core material, denoted T_{bt} is found to be a crucial parameter. If $T_{bt} > T_{fs}$, then the fracture modes of the bilayer structure can be predicted at any temperature T: for $T > T_{fs}$, the bilayer specimens just bend and for $T < T_{fs}$, they fail in a brittle way. If $T_{bt} < T_{fs}$, then the fracture modes of a bilayer structure can only be partially predicted: for $T > T_{fs}$, the bilayer specimens just bend and for $T < T_{bt}$, they fail in a brittle way.

However for $T_{bt} < T < T_{fs}$ the transition temperature, denoted T_{bts}, from a brittle fracture (and temporary arrest) to a permanent arrest cannot be explicitly predicted, and a model has to be developed. In this case the presence of the skin embrittles the structure more than a notch would, since for a temperature between T_{bt} and T_{bts} the notched core material is ductile whereas the un-notched bilayer structure is brittle.

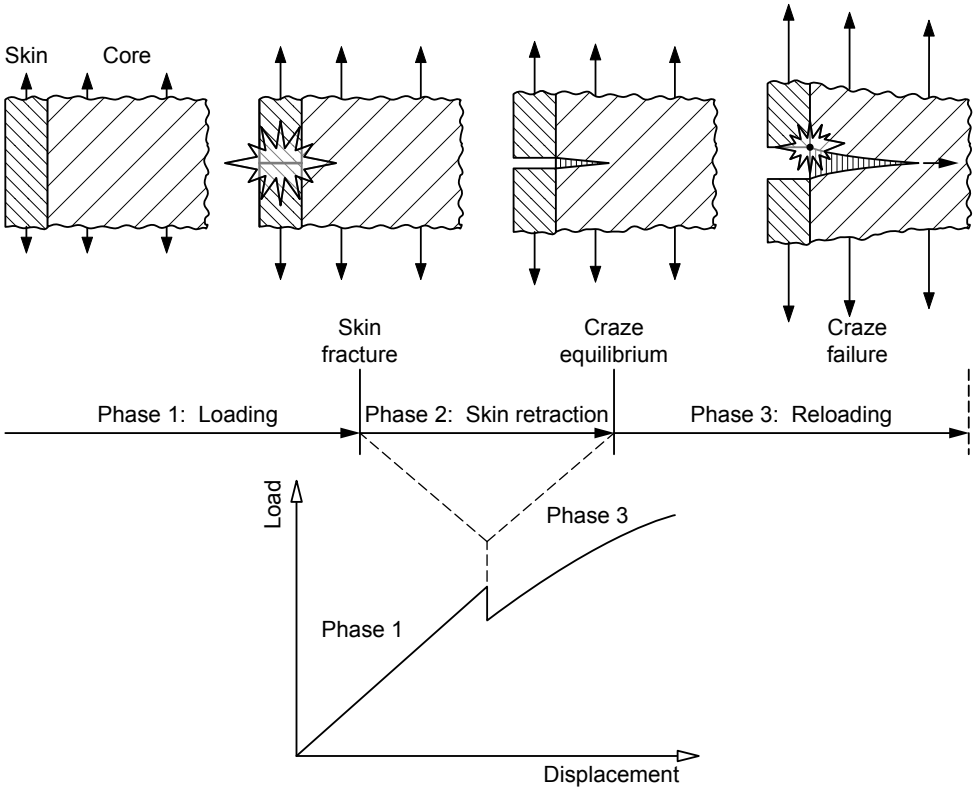

Fig. 5. Schematic of the three phases of the fracture of a bilayer structure and the associated load-displacement trace.

3 Model

On the basis of experimental observation, the fracture of a bilayer specimen is modelled as a three-phase process (Fig. 5). The first phase is the

quasi-static *loading* of the specimen: the un-notched specimen is bent until its surface strain reaches that for skin failure. The second, *skin retraction* phase begins with skin fracture — assumed to be instantaneous — and the appearance of a Dugdale-Barenblatt cohesive zone (i.e. a craze) to balance the strain singularity at the adjacent interface. As the skin ends retract the craze extends into the core material. This very localised dynamical process is responsible for much of the 'skin effect' through the very high imposed craze opening rate, (~100 m/s) although the corresponding unloading events observed in Fig. 2b, 2c and 3 appear to be relatively minor. The final *impact* phase is similar to impact loading of a monolayer specimen with a notch length equal to the skin thickness, except that the craze at the notch tip has already been heated by thermomechanical dissipation during the skin retraction phase. An adiabatic decohesion criterion will be therefore met sooner than if the skin had just been notched: this defines the phenomenon of embrittlement.

The criterion which determines whether the specimen fails by RCP is that of the adiabatic decohesion model (Leevers (1995)). The cohesive strength of this craze vanishes if thermomechanical heating at the active craze/bulk interface produces a melt layer of a thickness s_c which represents its structural size. There is no dissipation within the craze fibrils. This criterion differs from the critical-COD criterion of Romeo and Ballarini (1997), who modelled a crack-tip cohesive zone contacting a bilayer interface, in that bulk material properties determine its temperature and rate dependence. The phase during which the criterion is met determines the fracture mode: if it is reached during the skin retraction phase — before the crack opening rate $\dot{\delta}$ reaches zero — the specimen fails in a brittle way (Fig. 6a). If the criterion is met during the subsequent impact phase — before the load goes through a maximum — then there is a temporary arrest at the interface followed by RCP (Fig. 6b) and if the criterion is not met at the impact phase, then arrest at the interface is permanent (Fig. 6c).

The planar heat source q'' at each cohesive surface depends on the crack tip craze opening rate $\dot{\delta}$ and cohesive stress σ_c:

$$q'' = \beta \sigma_c \dot{\delta} \tag{1}$$

where β represents a thermomechanical efficiency. It generates very localised heating which is diffused by conduction, convected into the craze, and absorbed by phase transformation during melting of the material. Although originally formulated analytically, the adiabatic decohesion model was more recently implemented numerically by Leevers and Godart (2007), with fewer simplifying assumptions, using a one-dimensional finite volume formulation. The principal input to this procedure is a time history of crack tip craze opening displacement δ.

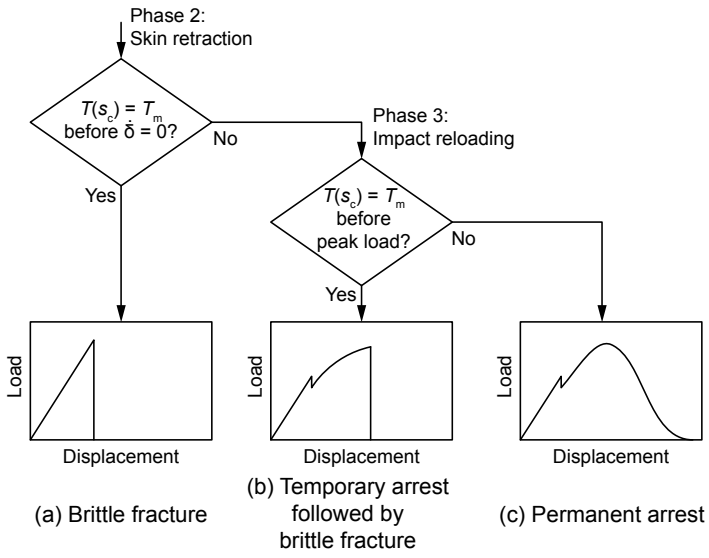

Fig. 6. Prediction of the fracture mode of a bilayer structure, depending on the phase at which the adiabatic decohesion criterion ($T(s_c) = T_m$) is met.

The initial speed of skin retraction is assumed to be unrestrained by the core material, so that the skin ends separate at a speed $2\epsilon_{fs}c_0$ where ϵ_{fs} is the skin failure strain and c_0 is the longitudinal wave speed in the skin, which depends on the skin modulus E_2 and density ρ_2 (the subscript 2 referring to the skin). The initial craze opening speed $\dot{\delta}_0$ is therefore

$$\dot{\delta}_0 = 2\epsilon_{fs}c_0 = 2\epsilon_{fs}\sqrt{\frac{E_2}{\rho_2}} \tag{2}$$

The retraction phase ends in the quasi-static state where the craze has reached its Dugdale size for the same striker displacement at which it appeared. Thus the duration of the retraction phase is considered negligible compared to that of the entire failure event — and it proves to be in the order of $\sim$1 μs over a total event time of 1 ms at 1 m/s. The calculation of this size, and the associated opening displacement δ_F is detailed in Appendix B. Between these end states, the craze opening rate is assumed to decrease linearly with time.

Observation of the fracture surface of notched Orgalloy specimens showed that the craze was long compared to other specimen dimensions, e.g. notch size. Therefore the assumption of a small craze length cannot be used here, and the quasi-static finite element method of Hayes and Williams (1972) was used to define craze size parameters. This method involves superposing a remote loading system (with no cohesive stress) and a uniform cohesive stress acting along the craze length (with no remote loading) such that the crack-tip singularity vanishes. This analysis (Appendix A) enables relationships between the COD at the interface δ, craze length c, force F at the impact point, and compliance C to be determined. Elastic

non-linearity of the material was also taken into account, by establishing a relationship between the modulus and the displacement of the striker according to Leevers and Morgan (1995), using tests on un-notched Orgalloy monolayer specimens. All these parameters are combined to determine the crack opening rate at each step of the finite-volume analysis (Appendix A).

4 Results

4.1 Validation of the program

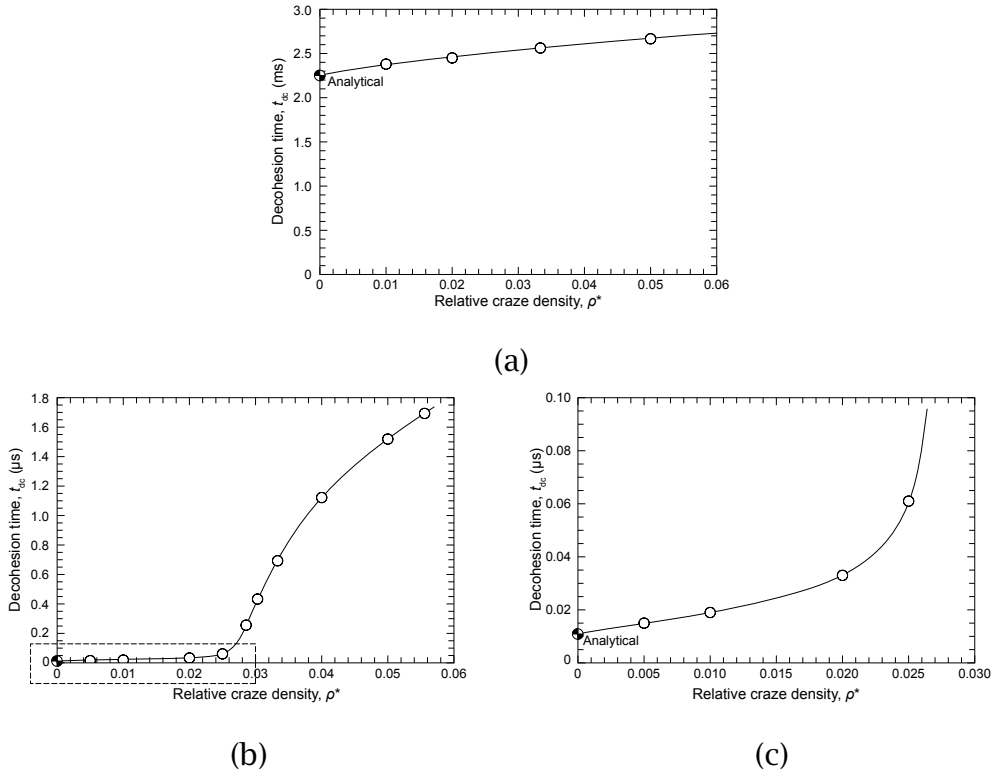

Fig. 7. Failure time as a function of craze density at 20°C during (a) impact on un-toughened Orgalloy with a notch of 0.6 mm, (b) skin retraction phase on un-toughened bilayer with 0.6 mm of EVOH and (c) detail of (b) around the origin. Square points on the y-axis are analytical results.

Although only the numerical implementation of the adiabatic decohesion model can give results when the relative craze density ρ^* is finite, analytical solutions can be derived when $\rho^* = 0$ and used as a reference. Analytical solutions for the impact reloading phase on a monolayer specimen have been fully described by Leevers and Godart (2007) and those during the skin retraction phase are derived in Appendix B. The computed

and analytical results are compared in Fig. 7: the convergence of the computed craze decohesion times t_{dc} towards the analytical values for a craze density of zero (square points on the y-axis) validates numerical method. For finite craze densities, the decohesion time increases, as heat is swept out into the craze. Figure 7 shows that the failure time of the impact phase is a few ms, whereas the skin retraction phase lasts around 1 μs, justifying treatment of the latter phase as instantaneous.

4.2 Cohesive stress

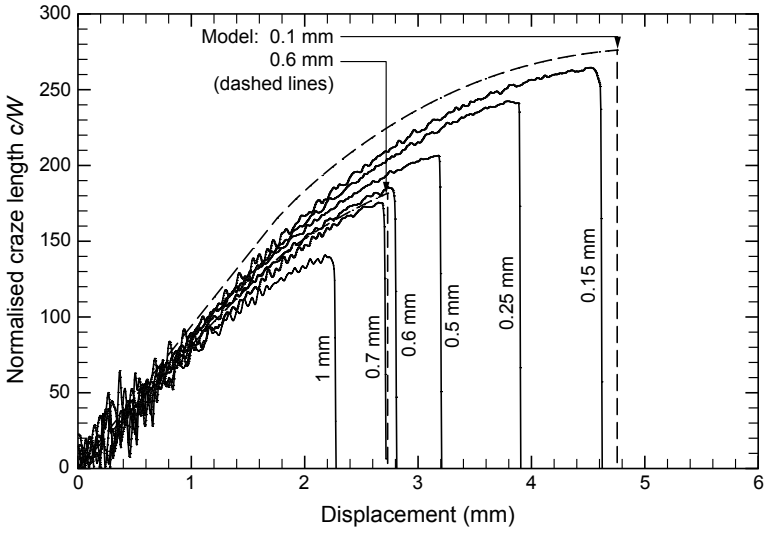

Fig. 8. Experimental and modelled load-displacement traces for notched un–toughened Orgalloy tested at 20°C and 1 m/s for various notch sizes.

The heat source in the adiabatic decohesion model (Eqn. 1) depends on the cohesive stress σ_c, a parameter which can be determined in several ways. Because σ_c determines the extent of craze growth and consequent softening of the specimen, it was determined here by comparing the modelled and experimental load-displacement traces for notched Orgalloy monolayer impact specimens. Experimental traces for un-toughened Orgalloy tested at 1 m/s and 20°C, are compared in Fig. 8 with those predicted for the cohesive stresses which gave the best fit (Table 4.2). These values are in very close agreement with those for yield stress at a strain rate of $\sim$10 s^{-1}, which is the strain rate obtained from TPB tests at 1 m/s on un-notched bilayer specimens (as seen in Fig. 3).

The final displacement (decohesion and failure) of the predicted load/displacement plot is affected by other parameter: thermomechanical efficiency β, critical thickness s_c and relative craze density $\rho^* = \lambda_F^{-1}$. These could therefore be adjusted until experimental and modelled traces agreed perfectly. However the precision of the model is limited by the repeatability of the exper-

Temperature ℃	Cohesive stress (MPa)	Yield stress (MPa)
20	65	55
0	72	70
-20	80	82

Table 1
Cohesive stress obtained by fitting the experimental and modelled load-displacement traces and yield stress from tensile tests

imental results: many tests carried out under exactly the same conditions will not give exactly the same load-displacement traces, and the fracture mode can also vary. Furthermore the same parameters should be used at various temperatures, for various notch sizes and for the toughened and un-toughened Orgalloy. They should therefore lead to a good agreement for all of these conditions.

Finally, the values of the parameters need to have the order of magnitude determined according to Leevers and Godart (2007): λ_F should lie between 10 and 20, β cannot exceed 0.9 and s_c should lie between 0.01 and 0.16 μm. In order to get the best agreement with the experimental traces with the chosen cohesive stress, the parameters were chosen so that the final displacement was the lowest, i.e. with the lowest fibril density ($\rho^* = 5\%$, hence $\lambda_F = 20$) and the highest thermomechanical efficiency ($\beta = 0.9$) and a low critical thickness of the melt layer ($s_c = 0.05\mu$m).

4.3 Temperature histories

Temperature histories in the active regions during impact on a notched monolayer specimen are shown in Fig. 9. The critical layer is so thin that its temperature distribution is only 1℃ lower than the temperature distribution of the cohesive surface. Therefore the melt layer thickens very soon after forming towards the end of the process. The slight decrease in temperature at 1.8 ms corresponds to the onset of elastic non-linearity, when the modulus starts to decrease (Fig. A.5 in Appendix).

Temperature histories in the active regions during the skin retraction phase of a bilayer specimen are shown in Fig. 10. The temperature of the cohesive surface increases rapidly at the beginning (the first temperature is actually already above the melting point) but then stabilises since the crack opening rate and hence the heat generated decrease and part of the heat source is used during melting of the material, as shown by the rapid increase of melt layer thickness. The temperature of the critical layer fol-

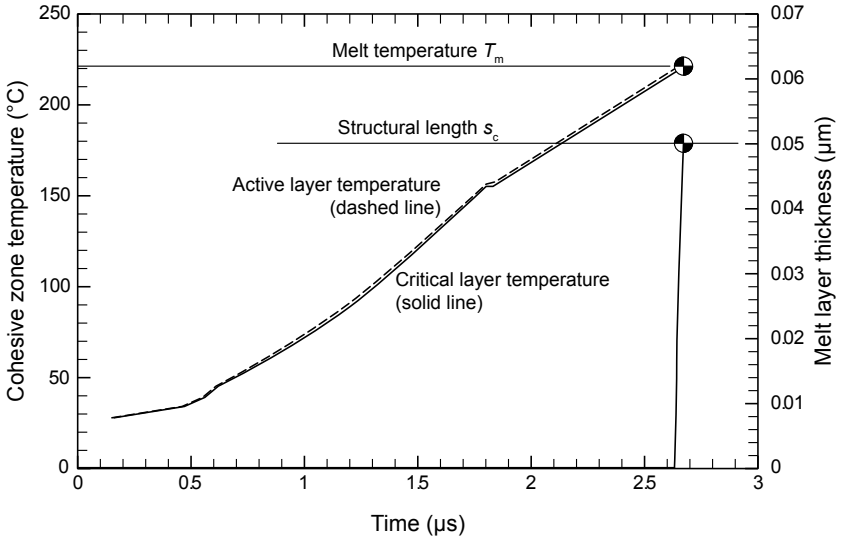

Fig. 9. Temperature and melt layer thickness histories in the active regions during the impact of an un-toughened Orgalloy specimen with a notch of 0.6 mm at 20°C at 1 m/s.

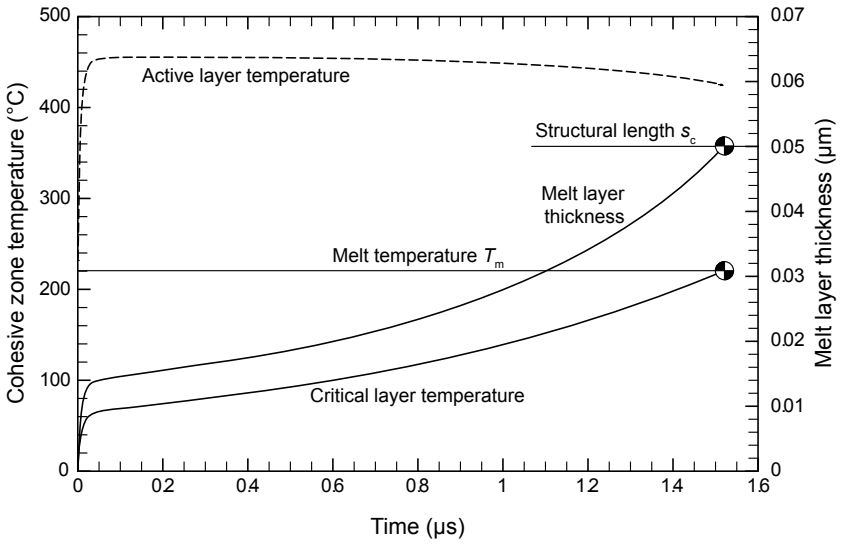

Fig. 10. Temperature and melt layer thickness histories in the active regions during the skin retraction phase of an un-toughened bilayer specimen with 0.6mm of EVOH at 20°C, with a failure strain of 3%.

lows the same sharp increase at the beginning and then the increase slows down.

Temperature histories in the active regions during the impact phase of toughened bilayer specimens with 0.1 mm of EVOH at 20°C are shown in Fig. 11. The peak corresponds to transfer of the temperature field from the skin retraction phase; the temperature of the critical layer was already close to the melting point. After the transfer, the temperatures decrease

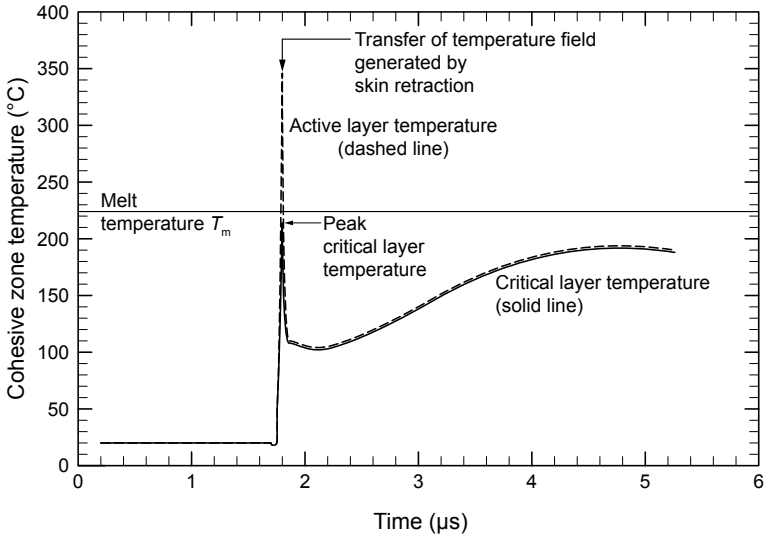

Fig. 11. Temperature histories in the active regions for the toughened bilayer specimens with 0.1 mm of EVOH at 20°C at 1 m/s

— since the hot material is drawn into the craze and the heat source generated by the impact is very low — and then they increase slowly during the impact process, as the crack opening rate and hence the heat source increase. The melting temperature is finally not reached at the end of the process, the adiabatic decohesion criterion is therefore not met.

4.4 Effect of skin failure strain

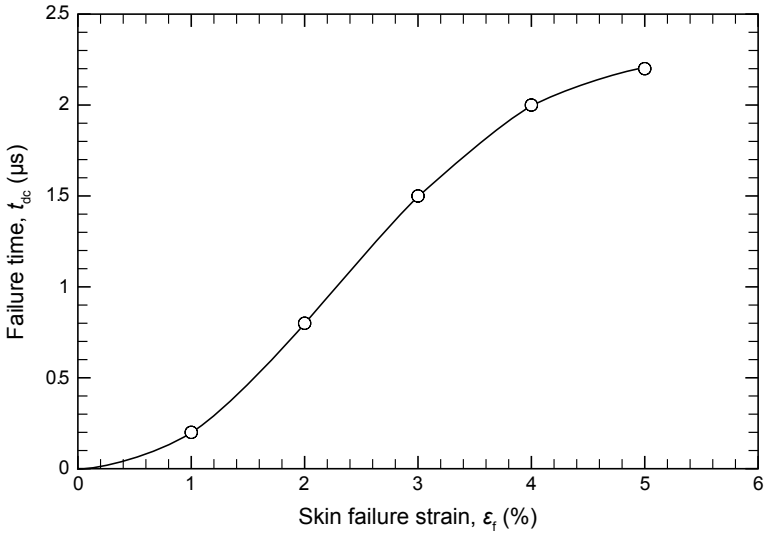

Fig. 12. Failure time for the un-toughened bilayer with 0.6 mm of EVOH at 20°C as a function of the failure strain of EVOH.

The initial crack opening rate $\dot{\delta}_0$ and final COD δ_F of the skin retraction

phase depend on the skin failure strain ϵ_{fs}, as shown in Table 2. The computed effect of failure strain on total decohesion time is shown in Fig. 12.

Failure strain ϵ_{fs} (%)	Initial crack opening rate $\dot{\delta}_0$ (m/s)	Final crack opening displacement δ_F (μm)
1	33	12
2	66	44
3	99	100
4	132	158
5	165	216

Table 2
Parameters defining the crack opening rate for different skin failure strains for the un-toughened bilayer with 0.6 mm of EVOH at 20°C

4.5 Comparison of the experimental and computed traces

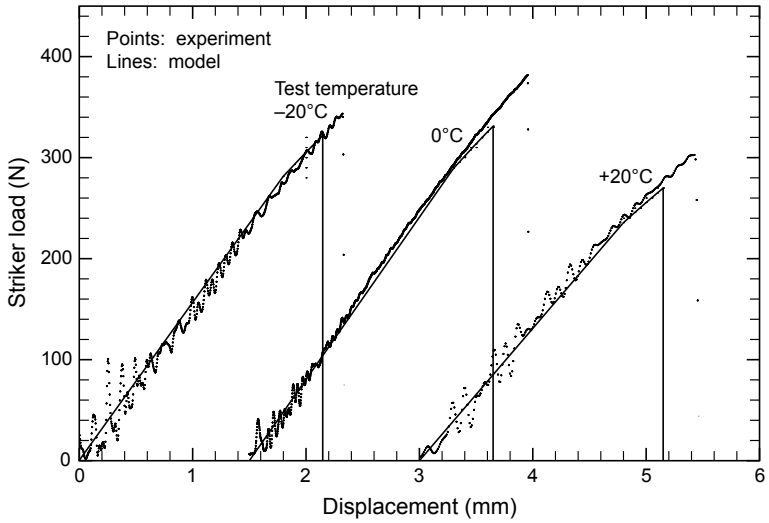

Fig. 13. Experimental and modelled load-displacement traces for un-toughened bilayer specimens with 0.6 mm of EVOH at 1 m/s and at 20, 0 and −20°C.

For the un-toughened bilayer with a 0.6 mm thick skin of EVOH, the adiabatic decohesion criterion is met during the skin retraction phase. The load-displacement trace is therefore defined only by the modulus of the bilayer beam (Fig. 13). The non-linearity that was determined by calculating the secant modulus for un-notched Orgalloy specimens is taken into account.

For the toughened bilayer specimens with 0.1 mm of EVOH at 0 and 20°C, the adiabatic decohesion criterion was not met, either during the skin

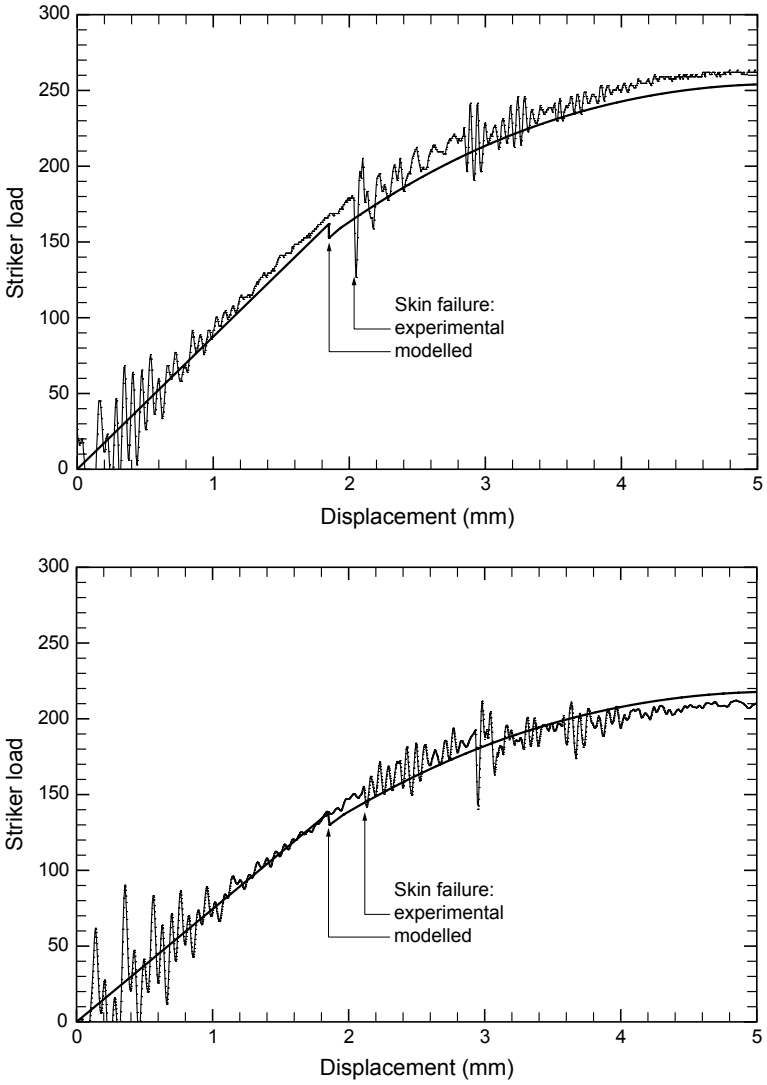

Fig. 14. Experimental and computed load-displacement traces for toughened bi-layer specimens with 0.1 mm of EVOH at 1 m/s and (a) 0 and (b) 20°C. Each experimental trace is only shown up to the maximum; in the remaining part of the trace, the load decreases steadily to zero.

retraction phase or during the impact. Therefore the crack formed in the EVOH skin was permanently arrested at the interface. The comparison of the experimental and computed load-displacement traces at 0 and 20°C are shown in Fig. 4.5. Figures 13 and 4.5 show very good agreement between the experimental and modelled traces.

5 Discussion

The model presented here expalins the skin embrittlement phenomenon in terms of a recognised failing of thermoplastics: relatively poor resistance to impact loading and rapid crack propagation. The model predicts whether a crack initiates in the skin layer and, if so, whether it then propagates through the whole structure or is arrested (either temporarily or permanently) at the interface. The fracture mode of the un-toughened bilayer structures with 0.1 and 0.6 mm of EVOH was found to be brittle at 1 m/s and the toughened bilayer with 0.1 mm of EVOH at 1 m/s was predicted to show permanent arrest. However this model cannot predict two other situations that were observed experimentally:

- multiple cracking, and
- arrest further away in the core material.

Multiple cracking corresponds to the situation where several cracks form and are arrested at the interface. An approach similar to the one developed by Kim and Nairn (2000) could be integrated to the model, where it is assumed that the next coating crack forms when the total energy released by the coating crack fracture event exceeds a critical value denoted as the *in-situ* fracture toughness of the coating. As for the arrest problem, the arrest properties of the core material, i.e. the fracture toughness at crack arrest have to be investigated further. This can be achieved by carrying out tests on a cracked ring which is subjected to a compressive load applied at its poles, while the crack is located on the equatorial plane at the outer surface of the specimen (Iung and Pineau (1996)). The main interest of this geometry lies in the variation of the stress intensity factor, with crack length, which follows a bell-shaped curve, numerically determined, the decreasing part defining crack arrest.

The failure strain of the skin material was found to be a crucial parameter and it should be determined more accurately, for example by carrying out tensile tests while observing the skin layer microscopically until the first crack appears, or by carrying out more tests with strain gauges. The reasons for choosing tensile tests are that it is easier to control the final position of the crosshead than it is during bending tests and the skin can be observed more easily from the side, whereas it is facing down during bending tests. However the crosshead speed should be adjusted so that the strain rate is the same as the surface strain rate in bending. The effect of the skin thickness on the skin failure strain should also be investigated. It would also be interesting to compare the failure strain obtained by testing the bilayer specimens to that obtained by testing a film of EVOH alone. It would be very useful to find a correlation between these two situations,

since the ultimate goal would be to predict the fracture mode of a bilayer structure using only experimental results from tests on monolayer specimens, thus eliminating the task of preparing bilayer structures.

The cohesive stress is another important parameter of the model. Additional data, e.g. the craze length, would enable it to be determined more accurately, reducing the number of undetermined parameters in the adiabatic decohesion model. In polyethylene a craze leaves a clear stress-whitened region on the fracture surface; in Orgalloy, though this whitened area was visible its limits were unclear. However the fact that the cohesive stresses determined were very close to the yield stresses validates the method used. Using directly the values of yield stress can therefore give a good approximation of the cohesive stress.

6 Conclusions

In order to predict the fracture mode of a bilayer structure, the brittle/ductile transition temperature of the core material, T_{bt}, with a notch size equal to the skin thickness, and the temperature of failure of the skin, T_{fs} have to be determined. If T_{bt} is greater than T_{fs}, then the fracture modes of the bilayer structure can be predicted at any temperature. Otherwise, the adiabatic decohesion model is used to predict the transition from brittle failure to permanent crack arrest for temperatures comprised between T_{bt} and T_{fs}. It requires the determination of the failure strain of the skin, and load-displacement traces on the notched core material should be recorded to determine the cohesive stress. The model predicts whether a crack initiates in the skin layer and then whether it propagates in the whole structure under RCP or whether it is arrested at the interface, either temporarily or permanently, and there was a very good agreement between the predictions and experimental results.

7 Acknowledgements

The authors gratefully acknowledge the financial support provided to Miss Godart by Arkema.

A Craze mouth opening rate during impact reloading

The parameters needed for numerical simulation, in addition to the thermal properties (k, h, C_p, ΔH_f and T_m) and the parameters of the adiabatic decohesion model (s_c, λ_F, β and σ_c) are:

- test temperature T_0,
- TPB specimen dimensions (W and B) and span S,
- Young's modulus of core E_1 and skin E_2 materials,
- skin thickness s,
- skin failure strain ϵ_{fs},
- skin density ρ, and
- crosshead speed.

At each step, calculation of the temperature distribution along the craze extension direction requires the craze opening rate to be a prescribed function of time (Eqn. 1). The bulk material along a line normal to the craze is divided into cells of size L_0 and at main time step one cell is drawn into the craze while being stretched by a fibril draw ratio λ_F. The craze opening rate at each step is therefore

$$\dot{\delta} = \frac{\lambda_F L_0}{\Delta t} \tag{A.1}$$

where Δt is the time elapsed during the step. The procedure for calculating the time t_j at the end of step j is as follows:

(1) A craze length is determined from the total crack opening displacement according to the Dugdale-Barenblatt criterion, using the superposition method described below.
(2) The force at the impact point of the TPB specimen and its compliance are determined from the craze length, using the same FE analysis results.
(3) The force and the compliance define a deflection.
(4) An effective secant modulus is associated with this deflection, accounting for large-deflection non-linearity.
(5) Steps 2 to 4 are repeated to convergence of the value of this modulus.
(6) The deflection is linked to the time by the crosshead speed.

Two specimens were modelled with skin thicknesses s of 0.1 and 0.6 mm (values of s/W of 0.025 and 0.15), but only the results for a skin thickness of 0.6 mm are presented here.

A.1 Superposition method

According to the Dugdale-Barenblatt model, the cohesive zone (craze) length is determined solely by the requirement to cancel the stress singularity at the crack tip. Several authors, including Hayes and Williams (1972) and Romeo and Ballarini (1997) used finite element analysis to determine the two elastic fields (Fig. A.1) whose singular parts must cancel. In the first 'remote loading' field, a remotely applied stress σ_r acts to open the crack. In the second 'cohesive' field, uniform tensile tractions σ_u acts over specified portions of length c of the crack face, the rest of the body being traction free.

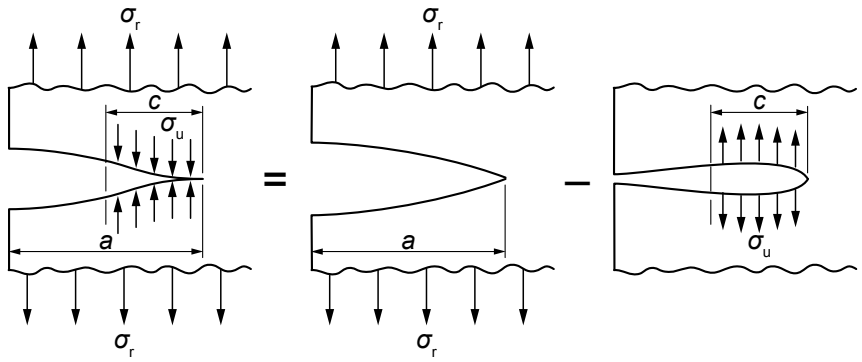

Fig. A.1. Superposition scheme for Dugdale model

The stress intensity factors K_{Ir} under remote loading were calculated for a range of crack lengths according to Eqn. A.2, where $r(a)$ is a numerically defined function of the crack length a.

$$K_{Ir} = r(a)\sigma_r\sqrt{a} \tag{A.2}$$

Then, for the same range of crack lengths in the cohesive configuration, the stress intensity factors K_{Iu} were determined according to Eqn. A.3, where $u(c,a)$ is a numerically defined function of a and the craze length c.

$$K_{Iu} = u(c,a)\sigma_u\sqrt{a} \tag{A.3}$$

The problem is then solved in the Dugdale model by requiring that the ratio of the stresses corresponding to both configurations is such that the stress intensity factors cancel (Eqn. A.4). Thus, with a and c defined, the corresponding ratio of stresses can be found.

$$\frac{\sigma_r}{\sigma_u} = \frac{u(c,a)}{r(a)} \tag{A.4}$$

The COD δ at a given temperature is obtained by subtracting the corresponding ratios of displacements under the two configurations, with a and c fixed. It is defined in Eqn. A.5, where δ_r is the COD in the remote loading configuration, δ_u corresponds to the uniform stress configuration, E_{mod} is the Young's modulus used in the modelling (E_{mod}=1 MPa was chosen for simplification), and E is the Young's modulus at the temperature considered.

$$\delta(c,a,T) = \left[\frac{\delta_r(a)}{\sigma_r}\frac{u(c,a)}{r(a)} - \frac{\delta_u(c,a)}{\sigma_u}\right] E_{mod}\frac{\sigma_c(T)}{E(T)} = \delta_0(c,a)\frac{\sigma_c(T)}{E(T)} \tag{A.5}$$

The calculation of remote stress as the surface stress of an un-notched beam is detailed in Eqns. A.6 to A.8, y_0 being the neutral axis of the beam (the subscript 1 refers to the core and 2 to the skin):

$$\sigma_r = \frac{E_2 FS}{4(EI)}(W - y_0) \tag{A.6}$$

$$\begin{aligned}(EI) = {} & E_1\left[\tfrac{1}{12}B(W-s)^3 + B(W-s)\left(y_0 - \tfrac{1}{2}(W-s)\right)^2\right] + \\ & E_2\left[\tfrac{1}{12}Bs^3 + Bs\left(W - \tfrac{1}{2}s - y_0\right)^2\right]\end{aligned} \tag{A.7}$$

$$y_0 = \frac{1}{2}\frac{(W-s)^2 + (E_2/E_1)(2W-s)s}{W + s\,(E_2/E_1 - 1)} \tag{A.8}$$

A.2 Dependence on the ratio of moduli

All the parameters obtained by FE analysis depend on the ratio of moduli E_2/E_1. This ratio remains almost constant from −20 to 20°C and is equal to 1.6 for un-toughened bilayer and 2.7 for toughened bilayer. The modelling was done for ratios in the range from 1 to 3 and the results were combined to get the parameters for any E_2/E_1 ratio. For a notch of 0.6 mm, a logarithmic relationship between the ratio of moduli and the parameters was found; Equation A.9 shows how the results of the ratio $u(c,a)/r(a)$ obtained for $E_2/E_1 = 1$ and $E_2/E_1 = 3$ were combined to predict the results for any E_2/E_1 ratio.

$$\left(\frac{u(c,a)}{r(a)}\right)_{E_2/E_1} = \frac{\ln(3E_1/E_2)}{\ln(3)}\left(\frac{u(c,a)}{r(a)}\right)_{E_2=E_1} + \frac{\ln(E_2/E_1)}{\ln(3)}\left(\frac{u(c,a)}{r(a)}\right)_{E_2=3E_1} \tag{A.9}$$

In the following paragraphs, the results of the modelling for $E_2 = E_1$ and $E_2 = 3E_1$ are presented for a skin thickness of 0.6 mm; for $E_2 = 2E_1$, the results of the modelling are compared with those predicted using Eqn. A.9.

A.3 Calculation of the craze length from the COD

Figure A.2 shows the relationships between the crack opening displacement and the craze length.

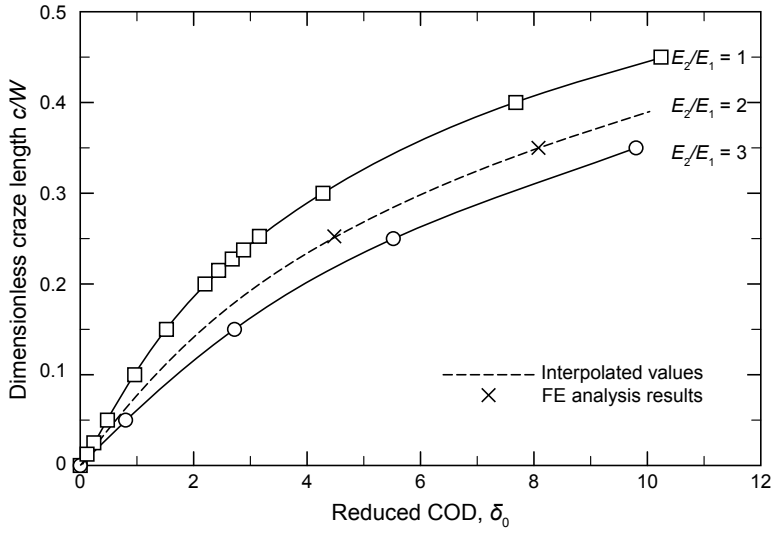

Fig. A.2. Determination of the craze length from the crack opening displacement for a bilayer with a 0.6 mm thick fractured skin for various ratios E_2/E_1. For $E_2/E_1 = 2$ the results of the analysis are compared to the predicted values from Eqn. A.2.

A.4 Calculation of the force from the craze length

The factor $u(c,a)/r(a) = \sigma_r/\sigma_u$, which yields the remote stress to generate a specified craze length for a specified cohesive stress $\sigma_u = \sigma_c$, also depends on the ratio of moduli E_2/E_1 (Fig. A.3). The force is then calculated according to Eqn. A.10.

$$F = \frac{4(EI)}{E_2 S(W - y_0)}\frac{u(c,a)}{r(a)}\sigma_c \tag{A.10}$$

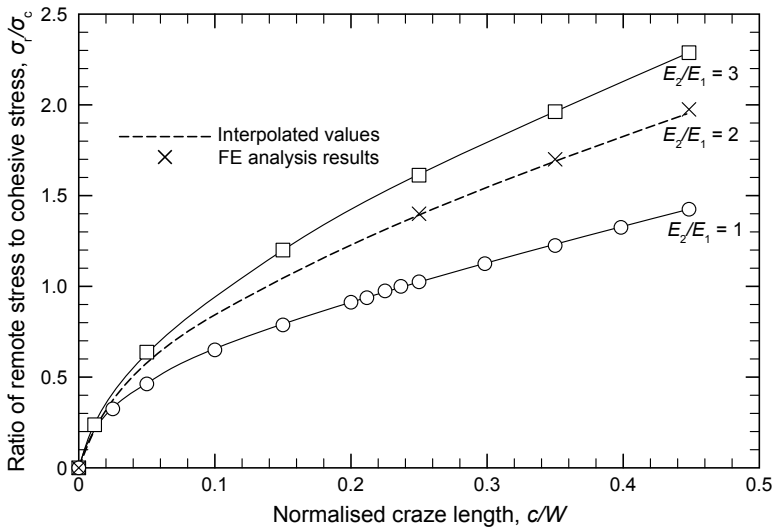

Fig. A.3. Ratio of the geometry functions $u(c,a)/r(a)$ for a bilayer with a 0.6 mm thick fractured skin for various values of E_2/E_1

A.5 Calculation of the compliance from the craze length

Figure A.4 shows the relationships between the non dimensional compliance $C^* = E'BC$ (C is the compliance and E' is the reduced modulus) and the craze length.

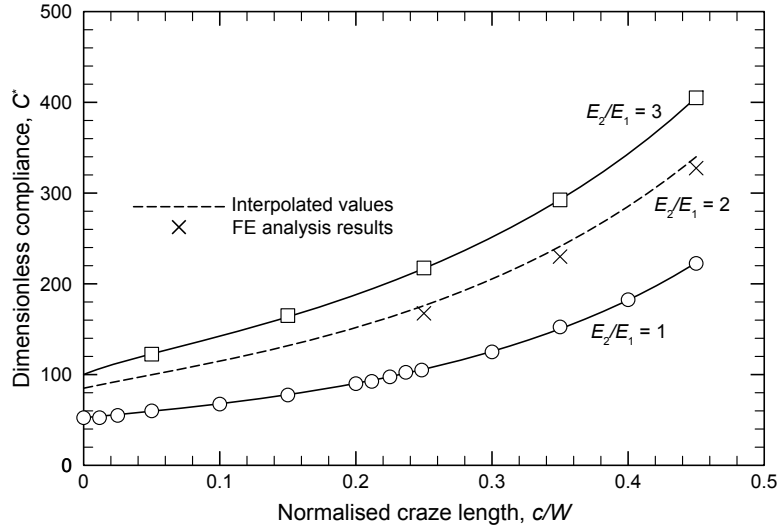

Fig. A.4. Determination of the non dimensional compliance from the craze length for a bilayer with a 0.6 mm thick fractured skin for various ratios E_2/E_1

A.6 Definition of a secant modulus

Leevers and Morgan (1995) used a classical 'pseudoelastic' approximation, in which the modulus is defined as a function of time at a similar strain rate to that imposed by the test. They found very good agreement between their model and experimental data from TPB tests on polyethylene grades.

The same approach is used here: TPB tests on un-notched Orgalloy were carried out and traces like the one of Fig. A.5 were obtained. Values of force P v.s. displacement d were collected (e.g. crosses on Fig. A.5) and an effective secant modulus E_{sec} was defined according to Eqn. A.11 (Leevers and Morgan (1995)).

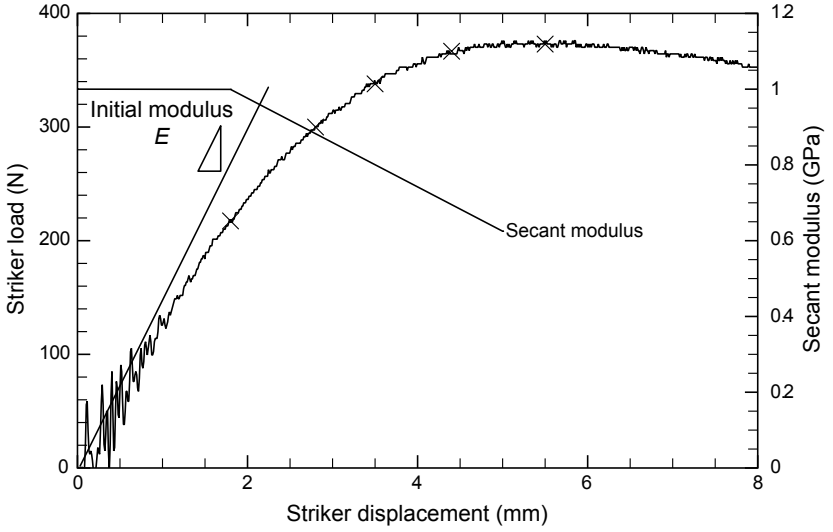

Fig. A.5. Load and secant modulus *vs.* displacement for un-toughened, un-notched Orgalloy in bending at 0°C

$$E_{\text{sec}} = \frac{P}{4dB}\left(\frac{S}{W}\right)^3\left[1 - 2.4(1+\nu)\left(\frac{W}{S}\right)^2\right] \tag{A.11}$$

The ratio E_{sec}/E, E being the elastic modulus, was determined as a function of displacement d (Fig. **??**). For displacements greater than 1.8 mm, which corresponds to the onset of non-linearity (Fig. **??**) this function was found to decrease linearly, and seemed to be independent of the temperature (from −20 to 20°C), test speeds (from 0.05 to 1 m/s) and Orgalloy type (toughened and un-toughened).

B Linear thermomechanical analysis for adiabatic heating during the skin retraction phase

The evolution of the temperature field at any distance z from the active layer, along the craze opening direction, is calculated using linear thermal conduction analysis (Eqn. B.1).

$$\Delta T(z,t) = \frac{1}{\rho C_{\mathrm{p}}(\pi\kappa)^{1/2}} \int_0^t \exp\left[-\frac{z^2}{4\kappa(t-u)}\right] \frac{q''(u)}{(t-u)^{1/2}} du \tag{B.1}$$

where κ is the thermal diffusivity $\kappa = k/\rho C_{\mathrm{p}}$, and t is the time. The heat source q'' depends on the crack opening rate, according to Eqn. 1; the crack opening rate is defined by Eqn. B.2.

$$\dot{\delta}(t) = -\frac{\dot{\delta}_0^2}{2\delta_{\mathrm{F}}} t + \dot{\delta}_0 \tag{B.2}$$

By changing the integration variable in Eqn. B.1 from u to $p^2 = \dfrac{t}{Fo}\dfrac{1}{(t-u)}$, where Fo is the Fourier number $Fo = \dfrac{4\kappa t}{z^2}$, the temperature distribution is

$$\Delta T(z,t) = \frac{\beta\sigma_{\mathrm{c}} z}{\rho C_{\mathrm{p}}\pi^{1/2}\kappa} \left(-\frac{(\dot{\delta}_0 z)^2}{12\delta_{\mathrm{F}}\kappa} \mathrm{I}(Fo) + \dot{\delta}_0 \mathrm{II}(Fo) \right) \tag{B.3}$$

where

$$\mathrm{I}(Fo) = Fo^{1/2}(Fo+1)\exp\left(-\frac{1}{Fo}\right) - \left(1+\frac{3}{2}Fo\right)\pi^{1/2}\,\mathrm{erfc}\left(\frac{1}{Fo^{1/2}}\right) \tag{B.4}$$

and

$$\mathrm{II}(Fo) = -\pi^{1/2} + \pi^{1/2}\,\mathrm{erf}\left(\frac{1}{Fo^{1/2}}\right) + Fo^{1/2}\exp\left(-\frac{1}{Fo}\right) \tag{B.5}$$

References

Cudre-Mauroux, N., Kausch, H. H., Cantwell, W. J., Roulin-Moloney, A. C., 1991. High speed crack propagation in bi-phase materials: an experimental study. International Journal of Fracture 50 (1), 67–77.

Djiauw, L., Fesko, D., 1976. Elongation of painted high-modulus elastomers at low temperatures. Rubber Chemistry and Technology 49, 1111.

Hayes, D. J., Williams, J. G., 1972. A practical method for determining dugdale model solutions for cracked bodies of arbitrary shape. International Journal of Fracture Mechanics 8 (3), 239–256.

Iung, T., Pineau, A., 1996. Dynamic crack propagation and crack arrest investigated with a new specimen geometry: 1. experimental and numerical calculations. Fatigue and Fracture of Engineering Materials and Structures 19 (11), 1357–1367.

Ivankovic, A., 1991. Rapid crack propagation in polymer multi-layer systems. Ph.D. thesis, Imperial College of London.

Kim, S. R., Nairn, J. A., 2000. Fracture mechanics analysis of coating/substrate systems. part i: Analysis of tensile and bending experiments. Engineering Fracture Mechanics 65 (5), 573–593.

Konczol, L., Doll, W., Ediger, B., 1991. On the mechanisms of surface embrittlement of ductile thermoplastics by brittle surface layers. In: Communications, I. (Ed.), 8th Deformation, Yield and Fracture of Polymers conference. Cambridge.

Leevers, P. S., 1995. Impact and dynamic fracture of tough polymers by thermal decohesion in a dugdale zone. International Journal of Fracture 73 (2), 109–127.

Leevers, P. S., Godart, M.-A., 2007. Adiabatic decohesion in a thermoplastic craze thickening at constant or increasing rate. submitted to: International Journal of Solids and Structures.

Leevers, P. S., Morgan, R. E., 1995. Impact fracture of polyethylene: a nonlinear-elastic thermal decohesion model. Engineering Fracture Mechanics 52 (6), 999–1014.

Romeo, A., Ballarini, R., 1997. A cohesive zone model for cracks terminating at a bimaterial interface. International Journal of Solids and Structures 34 (11), 1307–1326.

Schoolenberg, G. E., Meijer, H. D. F., 1991. Ultra-violet degradation of polypropylene: 2. residual strength and failure mode in relation to the degraded surface layer. Polymer 32 (3), 438–444.

So, P., Broutman, L. J., 1982. The effect of surface embrittlement on the mechanical behavior of rubber-modified polymers. Polymer Engineering and Science 22 (14), 888–894.

Theocaris, P. S., Milios, J., 1981. Crack-arrest at a bimaterial interface. International Journal of Solids and Structures 17 (2), 217–230.

Verpy, C., Gacougnolle, J. L., Dragon, A., Vanlerberghe, A., Chesneau, A., Cozette, F., 1994. The surface embrittlement of a ductile blend due to a brittle paint layer. Progress in Organic Coatings 24 (1-4), 115–129.